CHEMISTRY OF MATERIALS

pubs.acs.org/cm

Article

Seeded Growth of Three-Dimensional Block Heterojunctions Featuring Photoinduced Emission Enhancement

Yangyang Ren, Yanjun Gong,* Yanxue Che, Chenglong Liao, Hongwei Ji, Linfeng Cui,* Ling Zang, Yanke Che,* and Jincai Zhao

Cite This: *Chem. Mater.* 2024, 36, 6567−6574

Read Online

ACCESS | Metrics & More | Article Recommendations | Supporting Information

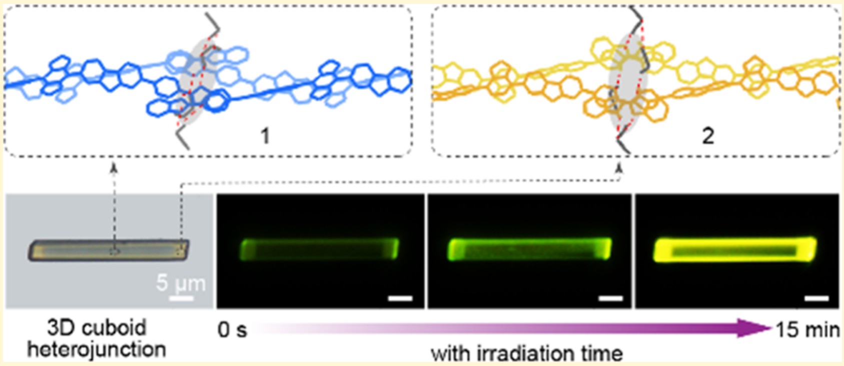

ABSTRACT: Three-dimensional (3D) block heterojunctions composed of different individual blocks may bring forth emergent properties beyond those of one-dimensional and two-dimensional block heterojunctions. However, the strategies to construct 3D block heterojunctions are still lack. Here, we report a living self-assembly of size-controlled 3D block heterojunctions that show remarkable photoinduced emission enhancement. A carefully designed near-infrared (NIR) donor−acceptor (D−A) molecule is assembled into a unique 3D architecture as a heteroseed. The NIR D−A molecules in this seed are circularly interconnected with 1-propanol through hydrogen bonding to create string-like building blocks, which are then packed laterally through electrostatic attraction and weak π-interactions into a 3D structure. The unique heteroseed can guide the continuous growth of another D−A molecule in the same manner to create a 3D block heterojunction with a nonphotostable outer block. Under ultraviolet irradiation, the intermolecular rearrangement of another D−A molecule can occur within the outer block, leading to an interfacial phase separation from the core block. The separation disrupts the efficient energy transfer from the outer block to the heteroseed core, thereby significantly enhancing the emission of the outer block. The utilization of heteroseed-guided self-assembly in the construction of photoresponsive 3D block heterojunctions represents a novel strategy for the advancement of photoresponsive functional materials.

1. INTRODUCTION

Organic heterojunctions of varying dimensions have wide applications in solar cells, lasers, diodes, and transistors.[1−9] However, research on three-dimensional (3D) organic heterojunctions predominantly concentrates on bulk heterojunctions, which are created using donor and acceptor molecules and are essential for the efficiency of organic photovoltaics.[1−4] By contrast, the construction of 3D block heterojunction architectures composed of different individual blocks, analogous to one-dimensional (1D)[10−18] or two-dimensional (2D) multiblocks,[19−23] remains largely unexplored. Given that 3D block heterojunctions likely possess unexpected optoelectronic properties beyond those of 1D and 2D heterojunctions, developing methodologies to create such 3D heterojunctions is of considerable interest in both fundamental and applied research.

Living seeded self-assembly represents a powerful methodology with an unparalleled control level for fabricating complex architectures.[24−36] To date, this strategy has allowed for the fabrication of various complex 1D and 2D multiblocks by using polymers and small molecules. However, living seeded self-assembly of 3D block heterojunctions remains an extreme challenge. The primary obstacle lies in the absence of heteroseeds that are suitable for cultivating 3D block heterojunctions. In response, we endeavored to create suitable

Received: March 25, 2024
Revised: May 27, 2024
Accepted: June 21, 2024
Published: June 28, 2024

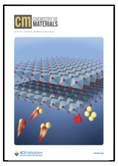

https://doi.org/10.1021/acs.chemmater.4c00874
Chem. Mater. 2024, 36, 6567−6574

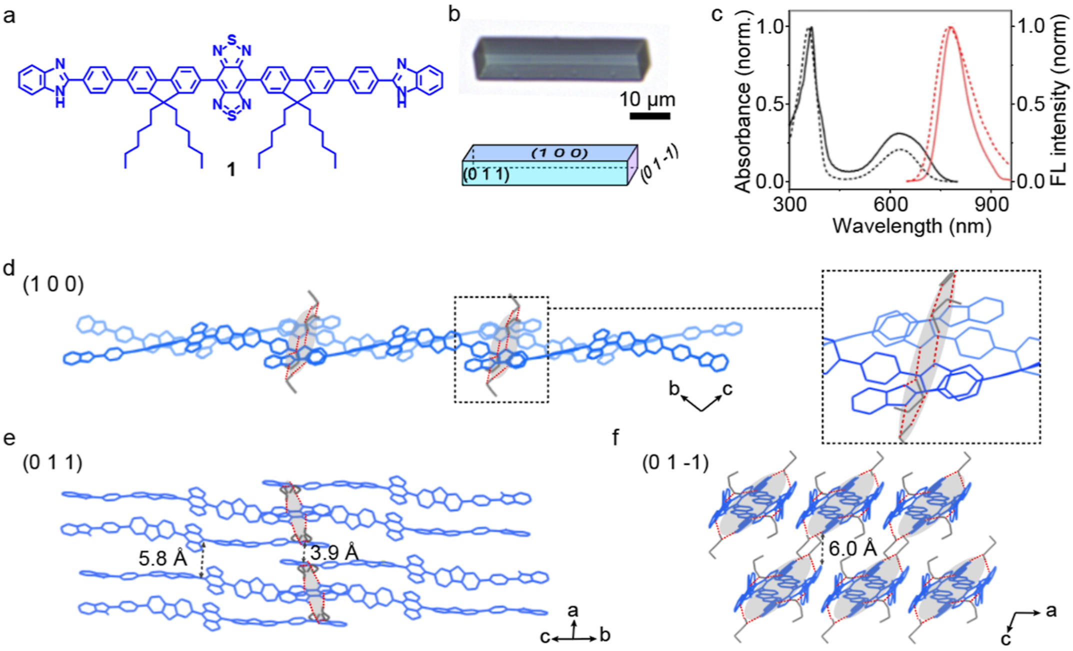

Figure 1. (a) Molecular structure of **1**. (b) Optical micrograph image of a cuboid crystal grown from **1** and its schematic illustration. (c) UV−vis absorption (black) and fluorescence spectra (red) of monomer **1** (4 μM) in toluene (dashed) and 3D cuboid crystals assembled from **1** placed on a glass slide (solid). (d−f) Molecular packing of **1** within a cuboid crystal, revealing different molecular interactions along different directions.

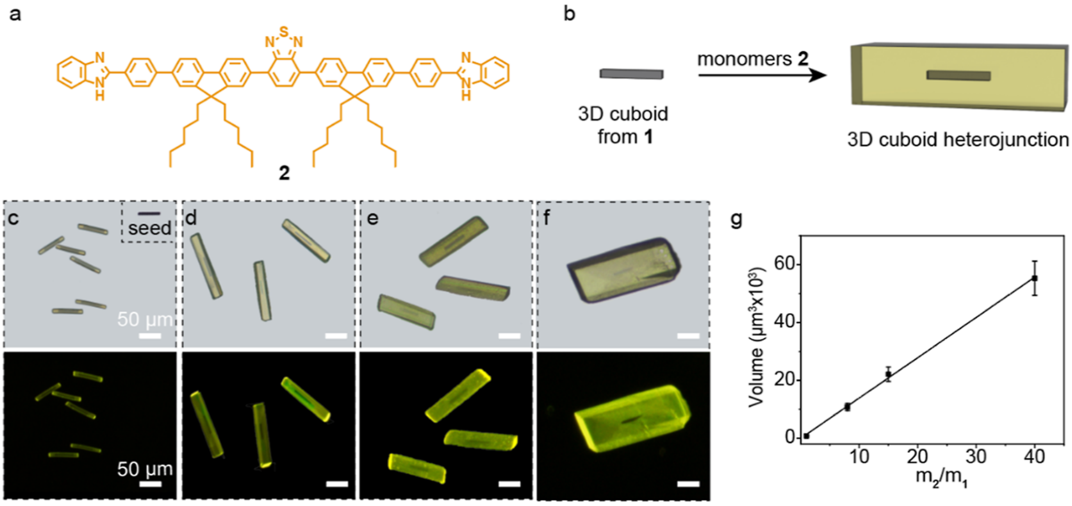

Figure 2. (a) Molecular structure of **2**. (b) Schematic representation of the seeded growth of the 3D block heterojunction composed of molecules **1** and **2**. (c−f) Bright-field and fluorescence-mode optical microscopic images of the 3D block heterojunctions with the outer blocks of different thicknesses, which were assembled upon the sequential addition of 0.1 mL of an acetonitrile solution of 3D cuboid crystals from **1** (0.05 mg/mL) into a supersaturated solution of **2** (0.1 mg/mL) in an acetonitrile/1-propanol (v/v, 5/1) mixture with varying volumes (0.05, 0.4, 0.75, and 2 mL) and aging at 25 °C for 30 min. This leads to the mass ratios of molecules **2** to molecules **1** (m_2/m_1) at (c) 1/1, (d) 8/1, (e) 15/1, and (f) 40/1. (g) Volume of the 3D block heterojunctions plotted as a function of the mass ratio of molecule **2** to molecule **1**.

3D molecular assemblies as heteroseeds and subsequently employed them for the growth of 3D block heterojunctions. In the present work, we report the development of a near-infrared (NIR) donor−acceptor (D−A) molecule **1** (Figure 1) and its organization into 3D cuboid crystals as heteroseeds. Single-crystal X-ray diffraction (SCXRD) analysis revealed that four molecules of **1** are interconnected in a circular manner with four 1-propanol molecules via hydrogen bonding (Figure 1). This arrangement extends into long string-like building blocks through circularly arranged hydrogen bonding and are subsequently laterally packed through electrostatic attraction and weak π-interactions forming 3D cuboid crystals (Figure 1). The unique 3D architecture can serve as a heteroseed to guide the packing of another D−A molecule **2** (Figure 2) in the same manner to form 3D block heterojunctions. Without the heteroseed, molecule **2** forms 1D structures with different molecular organization under the same assembly conditions, in stark contrast to the results observed with the heteroseed present. Interestingly, under ultraviolet (UV) irradiation, molecule **2** in the outer block undergoes a photoinduced intermolecular rearrangement, leading to interfacial phase separation in the 3D block heterojunction. The separation interrupts the efficient energy transfer from the outer block to the seed core (involving initial exciton diffusion within the outer block and energy transfer to molecule **1** at the interface), ultimately resulting in a notable emission enhancement of the outer block.

2. EXPERIMENTAL SECTION

2.1. Synthesis of Molecules 1 and 2. *2.1.1. Synthesis of Molecule 1.* ^{1}H NMR (400 MHz, tetrahydrofuran-d8, ppm): δ 11.8 (s, 2H), 8.33 (d, J = 8.0 Hz, 4H), 8.16 (d, J = 8.0 Hz, 2H), 8.08 (s, 2H), 8.02−7.94 (m, 8H), 7.89 (s, 2H), 7.83 (d, J = 8.0 Hz, 2H), 7.73 (d, J = 8.0 Hz, 2H), 7.51 (d, J = 8.0 Hz, 2H), 7.22 (d, J = 8.0 Hz, 2H), 2.51−2.24 (m, 8H), 1.35−1.14 (m, 24H), 0.96−0.93 (m, 8H), 0.84 (t, J = 8.0 Hz, 12H). MALDI-MS: (m/z) = 1243.4 (see details in the Supporting Information).

2.1.2. Synthesis of Molecule 2. Molecule **2** was synthesized by following the previously reported method.[21]

^{1}H NMR (400 MHz, tetrahydrofuran-d8, ppm): δ 11.83 (s, 2H), 8.31 (d, J = 8.0 Hz, 4H), 8.25 (s, 2H), 8.14 (d, J = 8.0 Hz, 2H), 8.06 (s, 2H), 8.00−7.92 (m, 8H), 7.87 (s, 2H), 7.81 (d, J = 8.0 Hz, 2H), 7.73−7.70 (m, J = 4.0 Hz, 2H), 7.50−7.47 (m, J = 4.0 Hz, 2H), 7.21−7.19 (m, J = 4.0 Hz, 4H), 2.25 (q, J = 2.0 Hz, 8H), 1.20−1.17 (m, 24H), 0.91−0.89 (m, 8H), 0.83−0.81 (m, J = 4.0 Hz, 12H). MALDI-MS: (m/z) = 1185.7.

2.2. Preparation of 3D Cuboid Crystals from 1 and 3D Block Heterojunctions from 1 and 2. *2.2.1. Size-Controlled 3D Cuboid Crystals Prepared via Living Seeded Self-Assembly of Only 1.* 3D cuboid crystals from **1** with a wide size distribution were prefabricated by injecting 0.1 mL of a 1-propanol/chloroform (v/v, 3/1) solution of **1** (0.5 mg/mL) into 1 mL of acetonitrile in a vial (4 mL) and aging at 25 °C for 24 h. Notably, chloroform herein was added to increase the solubility of **1** in the mixed solvent. The same procedure was used throughout this work if not otherwise specified. Irregular seeds were then prepared by sonicating the prefabricated 3D cuboid crystals suspended in acetonitrile at −30 °C for 1 min. Living self-assembly of the 3D cuboid crystals from only **1** with controlled sizes was performed by adding varying volumes (1, 0.25, 0.05, 0.0125, and 0.004 mL) of the resulting irregular seeds (0.005 mg/mL) in acetonitrile to a supersaturated solution of **1** (1 mL, 0.05 mg/mL) in an acetonitrile/1-propanol (v/v, 10/1) mixture, followed by aging at 25 °C for 30 min. The 3D cuboid crystals prepared using 0.0125 mL of the irregular seed solution were used as heteroseeds to grow the 3D block heterojunctions as follow.

2.2.2. 3D Block Heterojunctions Prepared via Living Seeded Self-Assembly. The 3D block heterojunctions with controlled sizes were prepared by adding 0.1 mL of acetonitrile solution of the heteroseeds (0.05 mg/mL) of **1** into varying volumes (0.05, 0.4, 0.75, and 2 mL) of a supersaturated solution of **2** (0.1 mg/mL) in an acetonitrile/1-propanol (v/v, 5/1) mixture, followed by aging at 25 °C for 30 min.

2.2.3. Bulk 3D Crystals of 1 and Block Heterojunctions Prepared for Single-Crystal Analysis. The bulk crystals of **1** with a size of at least 50 μm in each dimension were prepared by adding 1 μL of an acetonitrile solution of irregular seeds with particle sizes ranging from 400 nm to 3.8 μm into a supersaturated solution of **1** (2 mL, 0.05 mg/mL) in acetonitrile/1-propanol (v/v, 10/1) mixture and then aging at 25 °C for 2 days.

The bulk 3D block heterojunctions with a size of at least 50 μm in each dimension were prepared by adding 1 μL of an acetonitrile solution of the aforementioned heteroseeds of **1** into a supersaturated solution of **2** (2 mL, 0.1 mg/mL) in an acetonitrile/1-propanol (v/v, 5/1) mixture and then aging at 25 °C for 2 days.

2.2.4. 1D Structures Assembled from 2. 1D structures from **2** were prepared by injecting 0.1 mL of a 1-propanol/chloroform (v/v, 3/1) solution of **2** (0.5 mg/mL) into 0.5 mL of acetonitrile in a vial (4 mL) and aging at 25 °C for 24 h.

2.3. Property Characterizations. Fluorescence-mode optical microscopic images were obtained from an inverted fluorescence microscope with a NIR CCD detector (Olympus IX71). SCXRD measurements were carried out on a Rigaku XtaLAB PRO 007HF diffractometer equipped with graphite monochromatized Cu Kα (λ = 1.54184 Å) radiation in the ω scan mode. The structure was solved by intrinsic phasing (SHELXT) and refining by full-matrix least-squares on F2(SHELXL-2014). Powder XRD measurements were performed on a PANalytical X'Pert PRO instrument (40 kV, 200 mA). Scanning electron microscopy images were recorded on a Hitachi S-8010 and TESCAN MIRA LMS field-emission microscope. UV−vis spectra of 3D cuboid crystals from **1** were obtained using a UV−vis−NIR microscope (CRAIC Technologies, Inc.). The samples were drop-cast onto a glass substrate and dried in air. Fluorescence spectra of different 3D cuboid crystals were obtained on a Hitachi F-7000 fluorometer. Irregular seeds with small sizes were prepared using a commercial SCIENTZ-IID ultrasonic homogenizer at a power of 100 W.

3. RESULTS AND DISCUSSION

3.1. Molecular Design and Preparation of 3D Cuboid Crystals. In our prior research, we found that 2D structures can be formed from a D−A molecule through hydrogen bonding interactions between benzimidazole groups and alcohols, as well as electrostatic attraction between the D−A molecules.[21] We hypothesized that the compact bulk size of the benzothiadiazole group, along with its moderate electrostatic affinity among the D−A molecules, facilitated the formation of 2D structures. Conversely, we anticipated that increasing the bulk size of the A group and its electrostatic interactions among D−A molecules would result in the generation of a 3D architecture. With this hypothesis in mind, we synthesized a NIR D−A molecule **1**, incorporating a benzobisthiadiazole moiety with increased bulk size and electron-accepting ability instead of a benzothiadiazole group (Figure 1a), aiming to use it to create a 3D architecture. Upon injection of 0.1 mL of 1-propanol/chloroform (v/v, 3/1) solution of **1** (0.5 mg/mL) into 1 mL of acetonitrile in a vial (4 mL), 3D cuboid crystals of **1** (Figures 1b and S3) were indeed grown after aging at 25 °C for 24 h. Optical characterizations revealed that the 3D cuboid crystals have an NIR emission centered at 780 nm (Figure 1c). The NIR charge-transfer (CT) absorption is attributed to the increased electron-accepting capacity of the benzobisthiadiazole group. Furthermore, the spectral line width in the NIR emission of the 3D cuboid crystals is narrower than that of monomer **1** in toluene (Figure 1c). The broader fluorescence spectrum of monomer **1** in solution is likely attributed to the coupling of CT state vibration with solvation,[37,38] which enhances the degree of vibration freedom in the excited state compared to aggregates without the solvation effect. To gain insights into the molecular packing of **1** in the 3D cuboid crystal, SCXRD analysis was performed. As shown in Figure 1d, four molecules of **1** are alternatively connected at their benzimidazole ends with four 1-propanol molecules in a circular manner via hydrogen bonds to form a unique architecture, in which two molecules of **1** stretch out from each side of the connection circle. This arrangement extends into long string-like building blocks through circularly arranged hydrogen bonding. Simultaneously, the hydrogen-bond-linked architectures stack laterally in two dimensions, with an intermolecular distance of 5.8 Å in width and 6.0 Å in thickness, corresponding to electrostatic attraction (Figure 1e,f). Notably, weak π-interactions also exist along the width, as evidenced by the 3.9 Å spacing between the benzimidazole groups of **1** (Figure 1e). This organized architecture is also supported by the polarized emission from the 3D cuboid crystal, which suggests that the molecular orientation of **1** is generally parallel to the cuboid crystal long axis (Figure S4). In brief, the introduction of the bulky benzobisthiadiazole group leads to a unique circular hydrogen-bonding motif comprising four **1** molecules

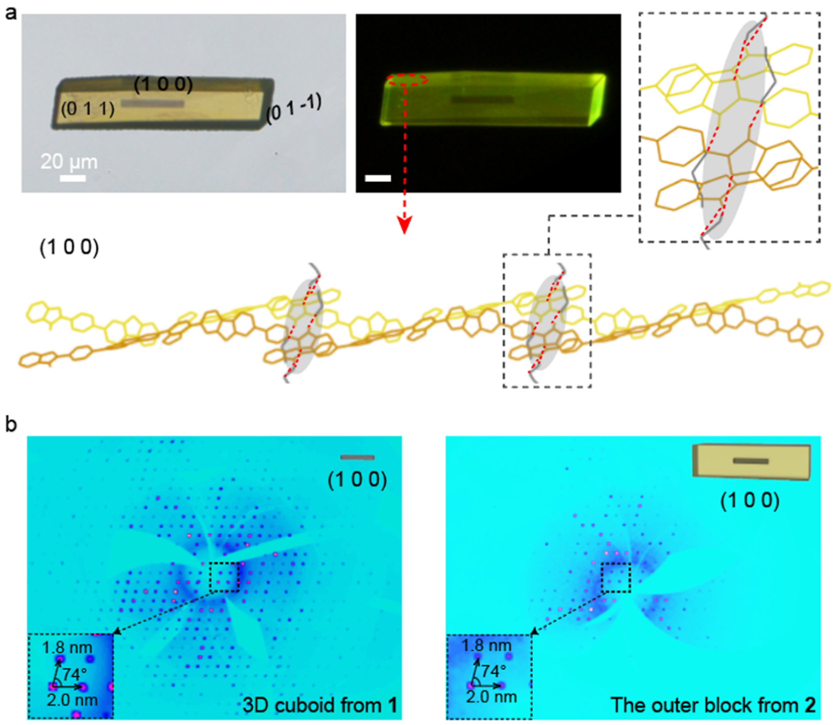

Figure 3. (a) Bright-field and fluorescence-mode optical images of a typical 3D block heterojunction and molecular packing of **2** within the 3D block heterojunction. (b) Diffraction spots observed through the (100) plane of a 3D cuboid crystal from a single molecule of **1** and of the outer block of a block heterojunction. Inset: magnified diffraction spots with *d*-spacing values correspond to the cell parameters along the *b* and *c* axes.

and four 1-propanol molecules. This motif extends and laterally packs via electrostatic attraction and weak *π*-interactions, ultimately forming a 3D cuboid crystal, as shown in Figure 1b.

3.2. Construction of 3D Block Heterojunctions. Having obtained the 3D cuboid crystals with unique molecular packing of **1**, we next investigated the possibility of seeded growth of 3D cuboid crystals with controlled sizes. Irregular seeds with particle sizes ranging from 400 nm to 3.8 *μ*m (Figure S5) were first prepared by sonicating prefabricated 3D cuboid crystals suspended in acetonitrile at −30 °C for 1 min. The XRD diffraction peaks of the prefabricated 3D cuboid crystals and irregular seeds of **1** largely coincide (Figure S6), indicating minimal changes in molecular packing as a result of the ultrasonic treatment. We utilized the new living self-assembly technique, which was recently developed to construct 2D structures in our laboratory,[35] to advance the seeded growth process. After adding varying volumes (1, 0.25, 0.05, 0.0125, and 0.004 mL) of seeds in acetonitrile (0.005 mg/mL) to the supersaturated solution of **1** (1 mL, 0.05 mg/mL) in an acetonitrile/1-propanol (v/v, 10/1) mixture, the living growth of the 3D cuboid crystals was monitored and recorded using optical microscopy. Notably, a supersaturated solution of **1** (0.05 mg/mL) in a mixture of acetonitrile/1-propanol (v/v, 10/1) was selected for its appropriate lag time of 3.5 h before spontaneous nucleation, as depicted in Figure S7. This extended preservation of **1** in its monomeric state facilitates subsequent seeded self-assembly processing. Figure S8 illustrates the formation of uniform 3D cuboid crystals, whose sizes are dependent on the monomer-to-seed mass ratios. Quantitative analysis revealed a linear relationship between the volumes of the 3D cuboid crystals produced and the monomer-to-seed mass ratios, as shown in Figure S8k. Furthermore, the diffraction peaks of the irregular seeds and heteroseeds of **1** are identical (Figure S6), indicating the epitaxial growth of molecule **1** on the seeds in a consistent manner. These observations indicate the living growth nature of the seeded self-assembly process.

Motivated by these observations, we subsequently utilized 3D cuboid crystals from **1** as heteroseeds to grow 3D block heterojunctions. Here, the D−A molecule **2** (Figure 2a) was selected because of the similarity of its molecular structure to that of **1**. Therefore, it is expected to be compatible with **1** to achieve seeded self-assembly, as shown in Figure 2b. Indeed, molecule **2** was heteroepitaxially grown on the heteroseeds of **1** to yield 3D block heterojunctions (Figure 2c−f). Both bright-field and fluorescence-mode optical images revealed the formation of a 3D block heterojunction in which a dark seed was embedded within the thick outer layer (Figure 2c−f). It should be noted that the seed remains dark simply because the camera used cannot detect NIR emission. Further analysis showed that the volumes of the 3D block heterojunctions produced are linearly dependent on the monomer-to-seed mass ratios of the added **2** monomers in relation to the seeds of **1**, as depicted in Figure 2g. This confirms the controlled heteroepitaxial growth achieved through the seeded self-assembly process. Notably, molecule **2** alone could not form such 3D architectures but formed microscale 1D structures under the same assembly conditions (Figure S9). The resulting 1D structures also exhibit distinct XRD results and fluorescence spectra compared to those of the 3D block heterojunction (Figure S10), indicating the different molecular packing when grown in the absence of seeds.

To investigate the molecular arrangement of molecule **2** within the 3D block heterojunction, SCXRD analysis of a bulk 3D block heterojunction (Figure 3a) was conducted. As shown in Figure 3a, molecule **2** adopts the same molecular packing motif as the seed, i.e., four molecules of **2** alternatively

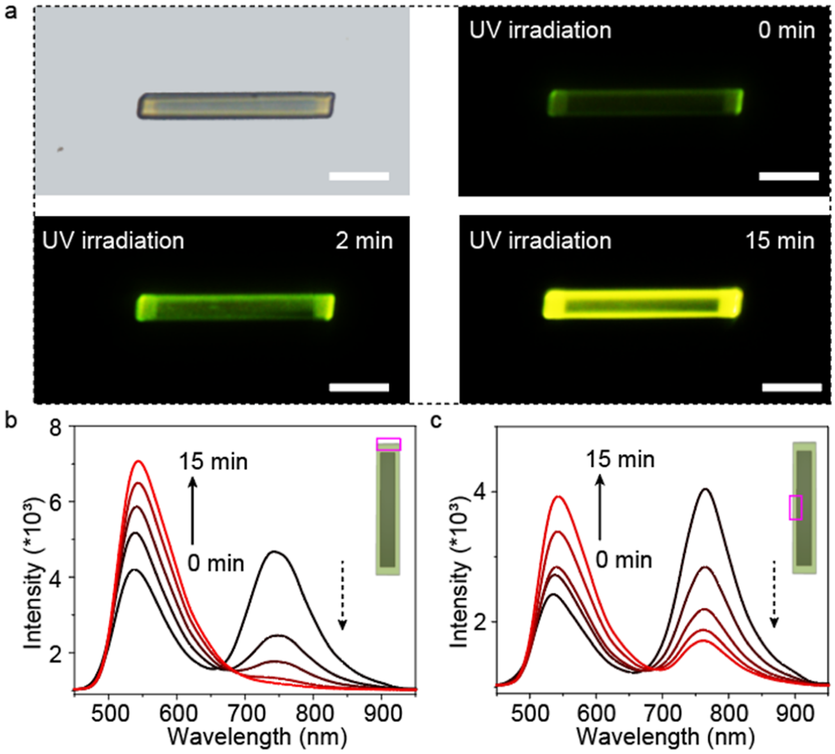

Figure 4. (a) Bright-field and fluorescence-mode optical images of a typical 3D block heterojunction under UV irradiation. Scale bars: 10 μm. (b,c) Fluorescence spectra with UV irradiation time monitored at the terminal (b) and the side (c) of the 3D block heterojunction.

connected at the benzimidazole ends in a circular fashion by four 1-propanol molecules via hydrogen bonds (Figure 3a and Table S1). The same molecular packing in the two blocks was also confirmed by their diffraction spots. The patterns observed through the (100) plane of a 3D cuboid crystal grown from only **1** and a block heterojunction are quite similar. Indeed, identical *d*-spacing values, corresponding to the cell parameters along the *b* and *c* axes, were calculated from the spots, as shown in Figure 3b. The results above enable us to conclude that the heteroseed's guiding effect facilitates the formation of 3D block heterojunctions. In these block heterojunctions, the unique molecular packing shared by molecules **1** and **2** is inaccessible to the conventional self-assembly of **2** alone.

3.3. Photoinduced Effect of 3D Block Heterojunctions. Because the molecular packing of **2** in the 3D block heterojunction is not driven by its inherent interactions but guided by the heteroseed, its molecular packing may be thermodynamically unstable. Given the potential for a significant rise in the dipole moment of D−A molecules following excitation,[39,40] we hypothesized that exposing molecule **2** to light might enhance its dipole−dipole interactions, potentially reducing the molecular arrangement of **2** in the 3D block heterojunction, thus leading to unanticipated photoresponsive characteristics. To verify this hypothesis, we applied UV light (330−390 nm) to irradiate the 3D block heterojunctions. Figure 4a shows that the emission from a typical 3D block heterojunction with the outer block of comparatively thin thicknesses gradually enhanced with irradiation time. This phenomenon is further evidenced by the fluorescence spectra recorded at the terminal and the side of a 3D block heterojunction, in which the fluorescence in the range of 500−650 nm assigned to **2** remarkably increases with irradiation time (Figure 4b,c). Simultaneously, the emission in the range of 730−850 nm ascribed to the seed from **1** decreases considerably (Figures 4b,c). The increase in fluorescence of **2** and the decrease in fluorescence of **1** under UV irradiation suggest that the initial energy transfer from **2** to **1** (Figure S11) is interrupted by a photoinduced effect, resulting in the restoration of the emission of **2**. In addition, the emission of 1D structures formed solely from molecule **2** (without the presence of seeds) was noted to decrease gradually over time under irradiation (Figure S12). This finding eliminates the likelihood of a straightforward photoreaction of molecule **2** as the cause of the heightened emission observed in the 3D block heterojunction mentioned earlier.

To gain detailed insights into the photoinduced effect, we next performed SCXRD measurements of the 3D block heterojunction after 30 min of UV irradiation. As shown in Figure S13 and Table S2, molecule **2** in the 3D block heterojunction retained the $P\bar{1}$ triclinic space group after irradiation but underwent a degree of shrinkage in the crystal cell. This resulted in noticeable photoinduced macroscopic crystal deformation, as illustrated in Figure S14. The diffraction spots of the outer block were also broadened after UV irradiation (Figure S15), indicating a decrease in the intermolecular distance of **2** upon photoillumination. The above results clearly point to a conclusion that the molecular packing of **2** guided by the heteroseed can undergo a photoinduced molecular rearrangement. In contrast, the cuboid crystals fabricated from only **1** exhibited no perceptible molecular rearrangement under identical UV irradiation, as evidenced by SCXRD analysis (Figure S16), which depicts the same molecular packing as that before UV irradiation. The enhanced photostability of the cuboid crystals fabricated from only **1** is ascribed to the larger size of the benzobisthiadiazole group in **1**, which results in steric hindrance to efficiently

https://doi.org/10.1021/acs.chemmater.4c00874
Chem. Mater. 2024, 36, 6567−6574

hinder the photoinduced molecular rearrangement. Conversely, the smaller size of the benzothiadiazole group is unable to withstand the increased dipole−dipole interactions of molecule **2** in the excited state, resulting in a contraction of the molecular packing. The differential photoresponsive behaviors of the outer block and the heteroseed are expected to induce interfacial phase separation (Figure S17). This separation would impede the energy transfer from excited molecule **2** to molecule **1** in the heteroseed, resulting in the previously mentioned enhancement of molecule **2**'s emission. It is important to note that a thermal stimulus, unlike UV light, cannot cause molecular rearrangement in 3D block heterojunctions. As demonstrated in Figure S18, the emission from a typical 3D block heterojunction with a thin outer block remains unchanged even with a temperature increase of up to 100 °C.

To further support the occurrence of photoinduced interfacial phase separation, we utilized UV light (330−390 nm) to irradiate 3D block heterojunctions with varying thicknesses of the outer blocks. As depicted in Figure S19, the fluorescence of **2** increased with irradiation time while the fluorescence of **1** decreased until the thickness of the outer block exceeded 750 ± 200 nm. Beyond this size point, a decrease in fluorescence was observed for molecules **2** and **1** as the irradiation time progressed (Figure S19d−g). The decrease is clearly attributed to the photobleaching effect. The thickness of approximately 750 nm aligns with the light absorption length of organic semiconductors, which is around 1 μm.[41] Below the threshold, light has the ability to penetrate the outer block and reach the interface. These observations, together with the optical and SCXRD analyses discussed above, lead to two specific conclusions. First, the decrease in the emission of the thick outer blocks, as shown in Figure S19d−g, rules out the possibility of the photoinduced emission enhancement of the thin outer blocks directly resulting from molecular reorganization. Second, upon reaching the interface of the 3D heterojunction, UV light induces a rearrangement that leads to interfacial phase separation. This phase separation disrupts energy transfer from the outer block to the seed core, consequently amplifying the emission of the outer block. In addition, the enhanced emission significantly surpasses the photobleaching effect.

4. CONCLUSIONS

In conclusion, we report the construction of size-tunable crystalline 3D block heterojunctions via living seeded self-assembly using two different D−A molecules (**1** and **2**) as building blocks. The NIR D−A molecule **1** enables the formation of a unique 3D architecture that contains a circular hydrogen-bonding motif composed of four D−A and four 1-propanol molecules. This unique 3D architecture can be used as a heteroseed to guide the heteroepitaxial growth of **2** to construct a 3D block heterojunction of different sizes, depending on the amount of **2** employed. The molecular packing of **2** in the outer block is directed by the heteroseed rather than the inherent molecular interactions of **2** itself. Consequently, the resulting structure is only metastable and has the ability to undergo photoinduced molecular reorganization when it is exposed to UV irradiation. The photoresponsive behavior induces interfacial phase separation within the 3D block heterojunctions, reminiscent of other photoresponsive properties observed in other organic crystals.[42−44] This separation disrupts energy transfer from the outer block to the seed, leading to a marked increase in the outer block's fluorescence. The application of heteroseed-guided self-assembly in the generation of photoresponsive 3D block heterojunctions opens up novel routes for the advancement of photoresponsive functional materials.

ASSOCIATED CONTENT

Supporting Information

The Supporting Information is available free of charge at https://pubs.acs.org/doi/10.1021/acs.chemmater.4c00874.

Synthesis of molecule **1**, ^{1}H NMR and MALDI-MS of molecule **1**, bright-field and fluorescence-mode optical microscopic images, and lattice parameters of the 3D cuboid crystal and 3D block heterojunction (PDF)

The single-crystal X-ray diffraction analysis of the 3D cuboid crystal from **1** (CIF)

The single-crystal X-ray diffraction analysis of 3D block heterojunction from **1** and **2** (CIF)

The single-crystal X-ray diffraction analysis of 3D block heterojunction from **1** and **2** after ultraviolet irradiation (CIF)

AUTHOR INFORMATION

Corresponding Authors

Yanjun Gong − *Key Laboratory of Photochemistry, CAS Research/Education Center for Excellence in Molecular Sciences, Institute of Chemistry, Chinese Academy of Sciences, Beijing 100190, China; School of Chemistry and Chemical Engineering, Shandong University, Jinan 250100, China;* orcid.org/0009-0005-6917-0707; Email: yjgong@sdu.edu.cn

Linfeng Cui − *Hebei Key Laboratory of Organic Functional Molecules, College of Chemistry and Material Science, Hebei Normal University, Shijiazhuang 050023, China;* Email: cuilinfeng@hebtu.edu.cn

Yanke Che − *Key Laboratory of Photochemistry, CAS Research/Education Center for Excellence in Molecular Sciences, Institute of Chemistry, Chinese Academy of Sciences, Beijing 100190, China; University of Chinese Academy of Sciences, Beijing 100049, China;* orcid.org/0000-0002-9671-3704; Email: ykche@iccas.ac.cn

Authors

Yangyang Ren − *Key Laboratory of Photochemistry, CAS Research/Education Center for Excellence in Molecular Sciences, Institute of Chemistry, Chinese Academy of Sciences, Beijing 100190, China; University of Chinese Academy of Sciences, Beijing 100049, China*

Yanxue Che − *HT-NOVA Co., Ltd., Beijing 101312, China*

Chenglong Liao − *Key Laboratory of Photochemistry, CAS Research/Education Center for Excellence in Molecular Sciences, Institute of Chemistry, Chinese Academy of Sciences, Beijing 100190, China; University of Chinese Academy of Sciences, Beijing 100049, China*

Hongwei Ji − *Key Laboratory of Photochemistry, CAS Research/Education Center for Excellence in Molecular Sciences, Institute of Chemistry, Chinese Academy of Sciences, Beijing 100190, China; University of Chinese Academy of Sciences, Beijing 100049, China*

Ling Zang − *Department of Material Science and Engineering, University of Utah, Salt Lake City, Utah 84112, United States;* orcid.org/0000-0002-4299-0992

Jincai Zhao – *Key Laboratory of Photochemistry, CAS Research/Education Center for Excellence in Molecular Sciences, Institute of Chemistry, Chinese Academy of Sciences, Beijing 100190, China; University of Chinese Academy of Sciences, Beijing 100049, China;* orcid.org/0000-0003-1449-4235

Complete contact information is available at: https://pubs.acs.org/10.1021/acs.chemmater.4c00874

Notes

The authors declare no competing financial interest.

ACKNOWLEDGMENTS

This work was funded by NSFC (nos. 21925604 and 22321004), the National Key Research and Development Program of China (nos. 2022YFA1205501 and 2019YFA0210401), and the Strategic Priority Research Program of Chinese Academy of Sciences (Grant no. XDB36000000).

REFERENCES

(1) Zhang, G. C.; Lin, F. R.; Qi, F.; Heumüller, T.; Distler, A.; Egelhaaf, H. J.; Li, N.; Chow, P. C. Y.; Brabec, C. J.; Jen, A. K. Y.; Yip, H. L. Renewed Prospects for Organic Photovoltaics. *Chem. Rev.* **2022**, *122* (18), 14180−14274.

(2) Lu, L. Y.; Zheng, T. Y.; Wu, Q. H.; Schneider, A. M.; Zhao, D. L.; Yu, L. P. Recent Advances in Bulk Heterojunction Polymer Solar Cells. *Chem. Rev.* **2015**, *115* (23), 12666−12731.

(3) Wadsworth, A.; Hamid, Z.; Kosco, J.; Gasparini, N.; McCulloch, I. The Bulk Heterojunction in Organic Photovoltaic, Photodetector, and Photocatalytic Applications. *Adv. Mater.* **2020**, *32* (38), 2001763.

(4) Wang, G.; Melkonyan, F. S.; Facchetti, A.; Marks, T. J. All-Polymer Solar Cells: Recent Progress, Challenges, and Prospects. *Angew. Chem., Int. Ed.* **2019**, *58* (13), 4129−4142.

(5) Peng, B. Y.; Wu, R. H.; Li, H. Y. Crystallization from a Droplet: Single-Crystalline Arrays and Heterojunctions for Organic Electronics. *Acc. Chem. Res.* **2021**, *54* (24), 4498−4507.

(6) Chandrabose, S.; Chen, K.; Barker, A. J.; Sutton, J. J.; Prasad, S. K. K.; Zhu, J. S.; Zhou, J. D.; Gordon, K. C.; Xie, Z. Q.; Zhan, X. W.; Hodgkiss, J. M. High Exciton Diffusion Coefficients in Fused Ring Electron Acceptor Films. *J. Am. Chem. Soc.* **2019**, *141* (17), 6922−6929.

(7) Ma, Y. X.; Yang, J.; Chen, S. H.; Lin, H. T.; Yan, C. C.; Zhuo, S. P.; Wang, X. D. Organic low-dimensional heterojunctions toward future applications. *Matter* **2022**, *5* (11), 3706−3739.

(8) Zhang, Y.; Liao, Q.; Wang, X. G.; Yao, J. N. A.; Fu, H. B. Lattice-Matched Epitaxial Growth of Organic Heterostructures for Integrated Optoelectronic Application. *Angew. Chem., Int. Ed.* **2017**, *56* (13), 3616−3620.

(9) Zhang, Y. J.; Dong, H. L.; Tang, Q. X.; Ferdous, S.; Liu, F.; Mannsfeld, S. C. B.; Hu, W. P.; Briseno, A. L. Organic Single-Crystalline p-n Junction Nanoribbons. *J. Am. Chem. Soc.* **2010**, *132* (33), 11580−11584.

(10) Zhang, W.; Jin, W. S.; Fukushima, T.; Saeki, A.; Seki, S.; Aida, T. Supramolecular Linear Heterojunction Composed of Graphite-Like Semiconducting Nanotubular Segments. *Science* **2011**, *334* (6054), 340−343.

(11) Jin, X. H.; Price, M. B.; Finnegan, J. R.; Boott, C. E.; Richter, J. M.; Rao, A.; Menke, M.; Friend, R. H.; Whittell, G. R.; Manners, I. Long-range exciton transport in conjugated polymer nanofibers prepared by seeded growth. *Science* **2018**, *360* (6391), 897−900.

(12) Zhang, D. D.; De, J. B.; Lei, Y. L.; Fu, H. B. Organic multicomponent microparticle libraries. *Nat. Commun.* **2021**, *12* (1), 1838.

(13) Kong, Q. H.; Liao, Q.; Xu, Z. Z.; Wang, X. D.; Yao, J. N. A.; Fu, H. B. Epitaxial Self-assembly of Binary Molecular Components into Branched Nanowire Heterostructures for Photonic Applications. *J. Am. Chem. Soc.* **2014**, *136* (6), 2382−2388.

(14) Zhu, X. T.; Yan, Y. J.; Sun, L. J.; Ren, Y. W.; Zhang, Y. H.; Liu, Y.; Zhang, X. T.; Li, R. J.; Chen, H. P.; Wu, J. S.; Yang, F. X.; Hu, W. P. Negative Phototransistors with Ultrahigh Sensitivity and Weak-Light Detection Based on 1D/2D Molecular Crystal p-n Heterojunctions and their Application in Light Encoders. *Adv. Mater.* **2022**, *34* (23), 2201364.

(15) Sarkar, A.; Behera, T.; Sasmal, R.; Capelli, R.; Empereur-mot, C.; Mahato, J.; Agasti, S. S.; Pavan, G. M.; Chowdhury, A.; George, S. J. Cooperative Supramolecular Block Copolymerization for the Synthesis of Functional Axial Organic Heterostructures. *J. Am. Chem. Soc.* **2020**, *142* (26), 11528−11539.

(16) Ma, X. J.; Zhang, Y. B.; Zhang, Y. F.; Liu, Y.; Che, Y. K.; Zhao, J. C. Fabrication of Chiral-Selective Nanotubular Heterojunctions through Living Supramolecular Polymerization. *Angew. Chem., Int. Ed.* **2016**, *55* (33), 9539−9543.

(17) Wan, Q. Y.; To, W. P.; Chang, X. Y.; Che, C. M. Controlled Synthesis of PdII and PtII Supramolecular Copolymer with Sequential Multiblock and Amplified Phosphorescence. *Chem* **2020**, *6* (4), 945−967.

(18) Chen, Y.; Wan, Q. Y.; Shi, Y. S.; Tang, B. T.; Che, C. M.; Liu, C. Three-Component Multiblock 1D Supramolecular Copolymers of Ir(III) Complexes with Controllable Sequences. *Angew. Chem., Int. Ed.* **2023**, *62* (50), No. e202312844.

(19) Lv, Q.; Wang, X. D.; Yu, Y.; Xu, C. F.; Yu, Y. J.; Xia, X. Y.; Zheng, M.; Liao, L. S. Lateral epitaxial growth of two-dimensional organic heterostructures. *Nat. Chem.* **2024**, *16*, 201.

(20) Sasaki, N.; Kikkawa, J.; Ishii, Y.; Uchihashi, T.; Imamura, H.; Takeuchi, M.; Sugiyasu, K. Multistep, site-selective noncovalent synthesis of two-dimensional block supramolecular polymers. *Nat. Chem.* **2023**, *15* (7), 922−929.

(21) Gong, Y. J.; Cheng, C. Q.; Ji, H. W.; Che, Y. K.; Zang, L.; Zhao, J. C.; Zhang, Y. F. Unprecedented Small Molecule-Based Uniform Two-Dimensional Platelets with Tailorable Shapes and Sizes. *J. Am. Chem. Soc.* **2022**, *144* (33), 15403−15410.

(22) Rajak, A.; Das, A. Crystallization-Driven Controlled Two-Dimensional (2D) Assemblies from Chromophore-Appended Poly(L-lactide)s: Highly Efficient Energy Transfer on a 2D Surface. *Angew. Chem., Int. Ed.* **2022**, *61* (15), No. e202116572.

(23) Qiu, H. B.; Gao, Y.; Boott, C. E.; Gould, O. E. C.; Harniman, R. L.; Miles, M. J.; Webb, S. E. D.; Winnik, M. A.; Manners, I. Uniform patchy and hollow rectangular platelet micelles from crystallizable polymer blends. *Science* **2016**, *352* (6286), 697−701.

(24) Ogi, S.; Sugiyasu, K.; Manna, S.; Samitsu, S.; Takeuchi, M. Living supramolecular polymerization realized through a biomimetic approach. *Nat. Chem.* **2014**, *6* (3), 188−195.

(25) Ogi, S.; Takamatsu, A.; Matsumoto, K.; Hasegawa, S.; Yamaguchi, S. Biomimetic Design of a Robustly Stabilized Folded State Enabling Seed-Initiated Supramolecular Polymerization under Microfluidic Mixing. *Angew. Chem., Int. Ed.* **2023**, *62* (34), No. e202306428.

(26) Fukaya, N.; Ogi, S.; Sotome, H.; Fujimoto, K. J.; Yanai, T.; Bäumer, N.; Fernández, G.; Miyasaka, H.; Yamaguchi, S. Impact of Hydrophobic/Hydrophilic Balance on Aggregation Pathways, Morphologies, and Excited-State Dynamics of Amphiphilic Diketopyrrolopyrrole Dyes in Aqueous Media. *J. Am. Chem. Soc.* **2022**, *144* (49), 22479−22492.

(27) Choi, H.; Ogi, S.; Ando, N.; Yamaguchi, S. Dual Trapping of a Metastable Planarized Triarylborane π-System Based on Folding and Lewis Acid-Base Complexation for Seeded Polymerization. *J. Am. Chem. Soc.* **2021**, *143* (7), 2953−2961.

(28) Gong, Y. J.; Fu, L. Y.; Che, Y. X.; Ji, H. W.; Zhang, Y.; Zang, L.; Zhao, J.; Che, Y. K. Fabrication of Two-Dimensional Platelets with Heat-Resistant Luminescence and Large Two-Photon Absorption Cross Sections via Cooperative Solution/Solid Self-Assembly. *J. Am. Chem. Soc.* **2023**, *145* (17), 9771−9776.

(29) Sleczkowski, M. L.; Mabesoone, M. F. J.; Sleczkowski, P.; Palmans, A. R. A.; Meijer, E. W. Competition between chiral solvents

and chiral monomers in the helical bias of supramolecular polymers. *Nat. Chem.* **2021**, *13* (2), 200−207.

(30) Weyandt, E.; ter Huurne, G. M.; Vantomme, G.; Markvoort, A. J.; Palmans, A. R. A.; Meijer, E. W. Photodynamic Control of the Chain Length in Supramolecular Polymers: Switching an Intercalator into a Chain Capper. *J. Am. Chem. Soc.* **2020**, *142* (13), 6295−6303.

(31) Weyandt, E.; Leanza, L.; Capelli, R.; Pavan, G. M.; Vantomme, G.; Meijer, E. W. Controlling the length of porphyrin supramolecular polymers via coupled equilibria and dilution-induced supramolecular polymerization. *Nat. Commun.* **2022**, *13* (1), 248.

(32) Khanra, P.; Singh, A. K.; Roy, L.; Das, A. Pathway Complexity in Supramolecular Copolymerization and Blocky Star Copolymers by a Hetero-Seeding Effect. *J. Am. Chem. Soc.* **2023**, *145* (9), 5270−5284.

(33) Moreno-Alcántar, G.; Aliprandi, A.; Rouquette, R.; Pesce, L.; Wurst, K.; Perego, C.; Brüggeller, P.; Pavan, G. M.; De Cola, L. Solvent-Driven Supramolecular Wrapping of Self-Assembled Structures. *Angew. Chem., Int. Ed.* **2021**, *60* (10), 5407−5413.

(34) Liu, Y.; Gong, Y. J.; Guo, Y. X.; Xiong, W.; Zhang, Y. F.; Zhao, J. C.; Che, Y. K.; Manners, I. Emergent Self-Assembly Pathways to Multidimensional Hierarchical Assemblies using a Hetero-Seeding Approach. *Chem.—Eur. J.* **2019**, *25* (59), 13484−13490.

(35) Liao, C. L.; Gong, Y. J.; Che, Y. X.; Cui, L. F.; Liu, Y. X.; Ji, H. W.; Zhang, Y. F.; Zang, L.; Zhao, J. C.; Che, Y. K. Living Self-Assembly of Metastable and Stable Two-Dimensional Platelets from a Single Small Molecule. *Chem.—Eur. J.* **2023**, *29* (72), No. e202301747.

(36) Ogi, S.; Stepanenko, V.; Sugiyasu, K.; Takeuchi, M.; Würthner, F. Mechanism of Self-Assembly Process and Seeded Supramolecular Polymerization of Perylene Bisimide Organogelator. *J. Am. Chem. Soc.* **2015**, *137* (9), 3300−3307.

(37) Painelli, A. Vibronic contribution to static NLO properties: exact results for the DA dimer. *Chem. Phys. Lett.* **1998**, *285*, 352−358.

(38) Terenziani, F.; Painelli, A.; Katan, C.; Charlot, M.; Blanchard-Desce, M. Charge Instability in Quadrupolar Chromophores: Symmetry Breaking and Solvatochromism. *J. Am. Chem. Soc.* **2006**, *128*, 15742−15755.

(39) Gong, Y. J.; Guo, Y. X.; Ge, F. Y.; Xiong, W.; Su, J.; Sun, Y.; Zhang, C.; Cao, A. M.; Zhang, Y. F.; Zhao, J. C.; Che, Y. K. Light-Driven Crawling of Molecular Crystals by Phase-Dependent Transient Elastic Lattice Deformation. *Angew. Chem., Int. Ed.* **2020**, *59* (26), 10337−10342.

(40) Cui, L. F.; Gong, Y. J.; Cheng, C. Q.; Guo, Y. X.; Xiong, W.; Ji, H. W.; Jiang, L.; Zhao, J. C.; Che, Y. K. Highly Photostable and Luminescent Donor-Acceptor Molecules for Ultrasensitive Detection of Sulfur Mustard. *Adv. Sci.* **2021**, *8* (4), 2002615.

(41) Najafov, H.; Lee, B.; Zhou, Q.; Feldman, L. C.; Podzorov, V. Observation of long-range exciton diffusion in highly ordered organic semiconductors. *Nat. Mater.* **2010**, *9* (11), 938−943.

(42) Awad, W. M.; Davies, D. W.; Kitagawa, D.; Mahmoud Halabi, J.; Al-Handawi, M. B.; Tahir, I.; Tong, F.; Campillo-Alvarado, G.; Shtukenberg, A. G.; Alkhidir, T.; Hagiwara, Y.; Almehairbi, M.; Lan, L. F.; Hasebe, S.; Karothu, D. P.; Mohamed, S.; Koshima, H.; Kobatake, S.; Diao, Y.; Chandrasekar, R.; Zhang, H. Y.; Sun, C. C.; Bardeen, C.; Al-Kaysi, R. O.; Kahr, B.; Naumov, P. Mechanical properties and peculiarities of molecular crystals. *Chem. Soc. Rev.* **2023**, *52* (9), 3098−3169.

(43) Yang, X. S.; Lan, L. F.; Li, L.; Yu, J. Y.; Liu, X. K.; Tao, Y.; Yang, Q. H.; Naumov, P.; Zhang, H. Y. Collective photothermal bending of flexible organic crystals modified with MXene-polymer multilayers as optical waveguide arrays. *Nat. Commun.* **2023**, *14* (1), 3627.

(44) Shields, D. J.; Karothu, D. P.; Sambath, K.; Ranaweera, R. A. A. U.; Schramm, S.; Duncan, A.; Duncan, B.; Krause, J. A.; Gudmundsdottir, A. D.; Naumov, P. Cracking under Internal Pressure: Photodynamic Behavior of Vinyl Azide Crystals through N2 Release. *J. Am. Chem. Soc.* **2020**, *142* (43), 18565−18575.